Advantages and Disadvantages of Computational Dosimetry Strategies in the Low mmWave Range: Comparison Between Multilayer Slab and Anthropomorphic Models

Micol Colella, *Member, IEEE*, Simona Di Meo, *Member, IEEE*, Micaela Liberti, *Senior Member, IEEE,* Marco Pasian, *Senior Member, IEEE,* Francesca Apollonio, *Senior Member, IEEE*

***Abstract*—Wireless technologies spanning at the higher bands of microwave range (i.e., Ka band) are gaining increasing importance in everyday life. Most recent Wireless Power Transfer (WPT) applications work in the microwave and millimeter wave (mmW) frequencies, overlapping with the new frequency bands of the fifth-generation mobile technology (5G). The spread of such novel electromagnetic (EM) sources raised the need to investigate their possible effects on population's health. Numerical dosimetry is fundamental to assess exposure of the human body. In the range 24 GHz – 28 GHz, i.e., the low-band spectrum of the mmW, and bridge between microwaves and mmW, there is poor consensus on the best strategy to model the human body. This paper proposes a comparison between the two numerical methodologies typically adopted for this frequency range: the use of multilayer planar slabs and realistic anthropomorphic numerical models. The aim is to highlight advantages and limits of each method, by comparing EM exposure results obtained on the ViP model Duke with several multilayer planar slabs. The differences between the two methods are non-negligible, suggesting the need of further studies and the necessity of improving both modeling approaches, depending on the frequency of work and the investigated application.**

***Index Terms*—5G technology, electromagnetic (EM) exposure, millimeter wave (mmW), multilayer slabs, numerical dosimetry, realistic anthropomorphic models, wireless power transfer (WPT)**

I. INTRODUCTION

IN A WORLD rapidly evolving, where smart environments based on object-to-human and object-to-object communications are increasingly spreading, the development of battery-free technologies is needed to facilitate several everyday life applications, such as medical and environmental monitoring, or intelligent transportation systems [1]–[3]. Wireless Power Transfer (WPT) has been recognized as the suitable solution to sustain energy supply in such applications, due to its ability to deliver electric energy without a direct contact between the power source and the load [4], [5]. The so-called far field (FF-)WPT systems can operate in the microwave (300 MHz – 30 GHz) and millimeter wave (mmW, 30 GHz-300 GHz) ranges [4], [6] and allow for long distance energy transfer [6], without requiring an accurate alignment between the transmitter and the receiver [1], [7], [8]. For such characteristics, FF-WPT has gained interest for application on implantable and wearable devices, in the frame of remote health control inside smart homes and smart hospitals [1], [9], [10].

An increasing number of studies is exploiting the mmW band for long-distance wireless power delivery, given the advantages in terms of size-reduction and high-power density [8], [11]–[13]. Thus causing the frequencies of application for FF-WPT to overlap with the higher frequency band of the emerging fifth-generation (5G) mobile technology, in a way that makes 5G dedicated technologies suitable for WPT applications [14].

The main effect of EM field exposure at the microwave and mmW frequency bands is tissue heating: the electromagnetic fields (EMFs) are absorbed superficially, due to the short power penetration depth [15], [16]. Exposure assessment at these frequencies typically requires to solve both the EM and the thermal problems, that extend over different distances scale: the RF energy focuses in the first millimeters of the body [16]–[18], while the heat propagates deeper inside the subcutaneous tissues and dissipates in the body core [16]. Consequently, the most relevant tissue for EM dosimetry at the mmW frequencies is the skin, which is anatomically composed by more layers, i.e., stratum corneum (SC), viable epidermis, dermis and hypodermis. The characteristics of each layer vary due to several factors, such as age, individual anatomy and body part, and the overall thickness of the skin can go from 0.5 mm to 3 mm [16], [19]. Furthermore, depending on the wavelength, the curvature radius of the body may be considered negligible. Given the aforementioned aspects regarding the exposure mechanism and the composition of the skin, the application of finite difference methods to realistic 3D anthropomorphic human models, typical of the RF dosimetry, has been abandoned in favor of simplified 1D multilayer planar slabs

This work has been developed in the framework of and supported by PRIN 2017 Wireless Power Transfer for Wearable and Implantable Devices (WPT4ID). *(Corresponding author: F. Apollonio).*

Micol Colella, is with the Department of Information Engineering, Electronics and Telecommunications (DIET), Sapienza University of Rome, Italy (e-mail: micol.colella@uniroma1.it).

Simona Di Meo and Marco Pasian are with the Department of Electrical, Computer and Biomedical Engineering, University of Pavia, Italy (e-mail: simona.dimeo@unipv.it, marco.pasian@unipv.it).

Micaela Liberti and Francesca Apollonio are with the Department of Information Engineering, Electronics and Telecommunications (DIET), Sapienza University of Rome, Italy and with the Center for Life Nano Science@Sapienza, Istituto Italiano di Tecnologia, Rome, Italy (e-mail: micaela.liberti@uniroma1.it, Francesca.apollonio@uniroma1.it).

Color versions of one or more of the figures in this article are available online at http://ieeexplore.ieee.org

[20]–[24]. The use of such simplified models has a first advantage in the reduction of the computational effort [25], [26]. Furthermore, currently available human body models [27], [28], are obtained from MRI data with 0.5 mm resolution, which intrinsically does not allow to identify the different skin layers, that can be as small as about 20 μm [16], [19]. Conversely, the planar slabs are able to reproduce the very first layers of the skin [16]. Nevertheless, this approach has drawbacks, because it can only be studied with a limited number of propagation directions in plane-wave exposure [26] and it is unable to describe the morphological features of the body, such as the curve shape of several body parts [29] or the cross-sectional tissue distribution [30], [31], whose effects on the exposure are still unclear [32]. Due to these aspects, there is no literature consensus on the best modeling approach to use for numerical exposure assessment, particularly in the range 24 GHz – 28 GHz [33]–[38].

This highlights the need of comparative studies in order to understand strengths and limitations of the two modeling approaches and build robust methodology for numerical exposure assessment. Hence, the aim of the present study is to perform a critical analysis on these two numerical approaches used in literature to assess EM exposure at 24 GHz.

To this aim three different body parts have been selected as a compromise between the curvature in the anatomical body shape and the practical positioning of wearable devices for health control: wrist (high curvature), arm (medium curvature) and back (low curvature). A comparison between the Duke model [27] and multilayer slabs is conducted showing that neglecting body shape and overall tissues distribution may lead to differences above 1 dB.

The paper is organized as follows. Section II gives an overview of the multilayer slab models typically proposed in literature to study human body exposure to an incident plane wave. Section III and IV describe the comparison between dosimetry on the Duke model and on two different typologies of multilayer slab models. Section V discusses the results, highlighting advantages and limitations of both the approaches.

II. Overview of the Planar Models Used in Literature

Modeling the first millimeters of the various anatomical regions as a slab of homogeneous layers on which a uniform plane wave impinges perpendicularly is typically used in the literature for dosimetric evaluations, especially in the millimeter-wave regime, due to the small wavelengths. Furthermore, the high values of signal attenuation allow limiting the analysis to the first few millimeters of tissue [20]–[23], [38]–[43]. At frequencies above 30 GHz, this approach can be applied to the sole skin, and requires to include the first layer of stratum corneum, without going deeper than the subcutaneous fat [44]. In the lower mmW range (i.e., 24 GHz-28 GHz) the stratum corneum has a negligible effect on the power absorption in skin [41], [44], and the heat propagates down to the extracutaneous tissues, [38], [41], [44] Therefore, depending on the frequency range of interest, the multilayer slab model should be accurately selected.

A summary of the typical multilayer (or multiplanar) slabs used in literature is reported in Table I.

In [42] and [43],the main dosimetric characteristics of the skin at frequencies above 30 GHz (e.g., reflection, power density, penetration depth, and SAR) are studied by considering two anatomical regions, characterized by two types of stratum corneum, thick and thin, which are wrist and forearm. Experimental reflection data are fitted using four skin models, one homogeneous, and three heterogeneous. Of these three, the first model is characterized by stratum corneum and skin tissue (2 layers), the second model by a sequence of stratum corneum, epidermis&dermis, and fat (3 layers), and the last model in which the stratum corneum is divided into outer and inner stratum corneum, a layer of epidermis&dermis, and finally a layer of fat (4 layers). The dielectric properties of the tissues used in these works were measured by the authors of [41] and [42].

In [20] and [39], Kanezaki et al studied the effect of dielectric permittivities on the increase in skin temperature due to the exposure above 30 GHz by modeling the human body as a slab of three uniform homogeneous layers, i.e., skin, fat, and muscle, on which a continuous plane wave impinges perpendicularly. In these works, dielectric properties of both the skin and the infiltrated fat were derived by [45].

The same sequence of layers (skin, subcutaneous fat tissue and muscle) was used by Wu et al in 2015 [40] to model human tissue with the aim of analyzing the steady-state temperature increase due to the exposure to EM waves at 40 GHz, 60 GHz, 80 GHz and 100 GHz. Also in [40], as in previous works, a uniform plane wave with propagation direction normal to the tissue surface is assumed. In this work, the dielectric properties of all the tissues were derived by [44].

Sasaki et al, on the other hand, in [21], derived a computational model for dosimetric evaluations considering the penetration depth of EM waves, from microwaves to THz (10 GHz – 1 THz). Specifically, from considerations based on the penetration depth within the skin and the wavelength, they derive a four-layer model that includes the epidermis, dermis, subcutaneous tissue, and muscle. Again, a plane wave with normal incidence on the surface of the skin layer is considered. The dielectric properties of the tissues used in this work were measured by the same authors [21].

In [44], calculations of reflection, power deposition and heating of the skin exposed to EM radiation in the frequency range 6-100 GHz are made by considering two models of the skin consisting of 3 or 4 layers. The 3-layer model includes stratum corneum, viable epidermis&dermis, and subcutaneous fat, and the 4-layer one in which muscle is added to the previously described model. The dielectric properties of the skin were derived by [41] and [42], while the dielectric properties of both the infiltrated fat and the muscle were derived by [45]. In [22], with the aim of establishing the relationship under various exposure conditions, the authors consider obliquely incident electromagnetic waves for frequencies from 6 GHz to 1 THz on a 4-layer skin model consisting of epidermis, dermis, fat and muscle. The dielectric properties of

TABLE I
GEOMETRICAL PROPERTIES OF MULTIPLANAR BODY MODELS AVAILABLE IN LITERATURE

	Stratum Corneum	Epidermis	Dermis	Fat	Muscle
	d (mm)	d (mm)	d (mm)	d (mm)	d (mm)
Alekseev et al., 2007 [42]	-	inf			-
	0.015mm	inf			-
	0.015 mm	1.45 mm		inf	-
	0.43 mm	inf			-
	0.42 mm	1.85 mm			-
	0.43 mm; 0.05 mm	1.8 mm		inf	-
Alekseev et al., 2008 [43]	-	inf			
	0.15 mm	inf			
	0.015 mm	1.45 mm		inf	
	0.43 mm	inf			
	0.42 mm	1.85 mm			
Kanezaki et al., 2008 [20]	1 mm			3 mm	31 mm
Kanezaki et al., 2009 [39]	1 mm			3.5 mm	55.5 mm
Wu et al., 2015 [40]	1 mm			3 mm	31 mm
Sasaki et al., 2017 [21] & Li et al., 2019 [22]	-	0.102±0.034 mm	1.08±0.16 mm	3.89±1.40 mm	23.3±4.3 mm
	-	0.0835±0.0362 mm	1.03±0.33 mm	8.65±4.28 mm	34.8±10.5 mm
	-	0.0948±0.0236 mm	1.22±0.32 mm	9.35±4.17 mm	50.5±4.2 mm
	-	0.0794±0.0339 mm	1.25±0.26 mm	14.3±7.5 mm	14.4±3.5 mm
Ziskin et al., 2018 [44]	0.015 mm	1.45 mm		Inf (3-layer model); 1 - 6 mm (4-layer model);	none (3-layer model); Inf (4-layer model);
Christ et al., 2020 [23]	0.02-0.7 mm*; 0.01-0.02 mm**	0.06-1.2 mm	0.4-2.4 mm	Inf (3-layer model); 1.1-5.6 mm	none (3-layer model); Inf (4-layer model);
Sacco et al., 2021 [41]	0.015 mm	1.396 mm	0.06 mm	4 mm	inf

* Thick skin: Palm and soles
** Thin skin: rest of the body

the tissues used in this work were measured by the same authors [21].

In [23], wave reflection and temperature rise induced by the EM field between 6 and 100 GHz are studied using a stratified skin model under the normal incidence condition of plane wave. The skin in this study is modeled as a layered planar structure composed of four or five layers of different tissues, characterized by different degrees of perfusion: the stratum corneum and viable epidermis, both of which are not perfused, the dermis, i.e., the outermost perfused skin layer, the adipose tissue subcutaneous (perfused), and the muscle. This last layer, however, is included only in configurations in which reflections from the fat-muscle interface are also considered. The tissues dielectric properties were the same as [43].

between power density and skin surface temperature increase

Recently, in 2021, Sacco et al. [41] evaluated the effect of age on dosimetric characteristics such as power density, SAR and tissue heating near the surface, considering two exposure frequencies, 26 GHz and 60 GHz. Again, the incidence is a uniform plane wave that affects the stratification perpendicularly. In this work, the authors conduct both EM and thermal analysis over a four layer body model composed by two skin layers (stratum corneum and epidermis&dermis), one layer of fat, representing the subcutaneous fat, and one layer of muscle. The two skin layers are characterized by different percentages of water and, therefore, have a greater or lesser impact on EM or thermal analysis. In particular, the stratum corneum has negligible water content, so it has no significant impact on power absorption in the skin, while epidermis and dermis from the EM point of view can be considered the same layer, because they have about the same amount of water, although they have different heat dissipation capacity, since the dermis contains blood vessels. In [40], the dielectric properties of the SC were derived by [43], while those of the dry skin, non infiltrated fat and muscle from [45]. From these past works it emerged that when studying frequencies above 30 GHz, extracutaneous layers such as the muscle can be neglected and the analysis focuses on the skin, modeled as a sequence of

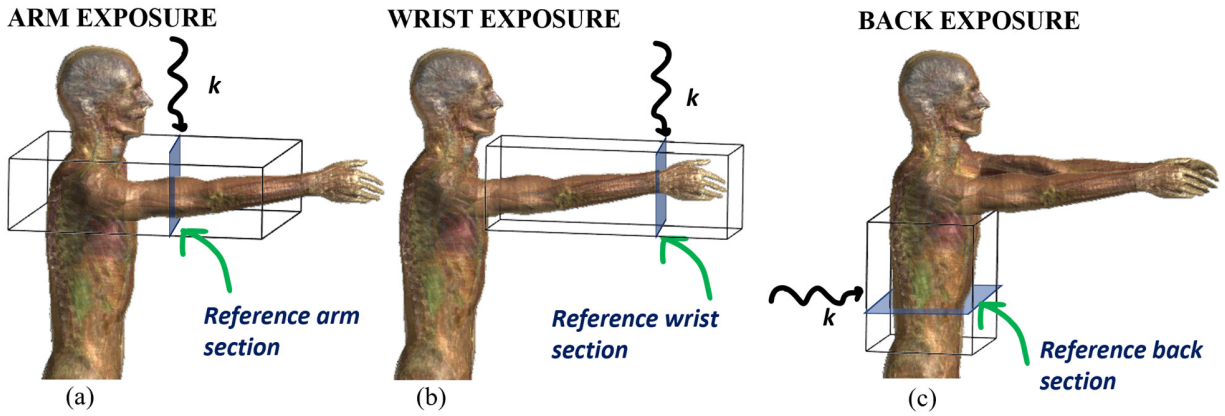

Fig. 1 Exposure of the virtual human body model Duke: (a) Plane wave impinging on the arm. (b) Plane wave impinging on the wrist. (c) Plane wave impinging on the back.

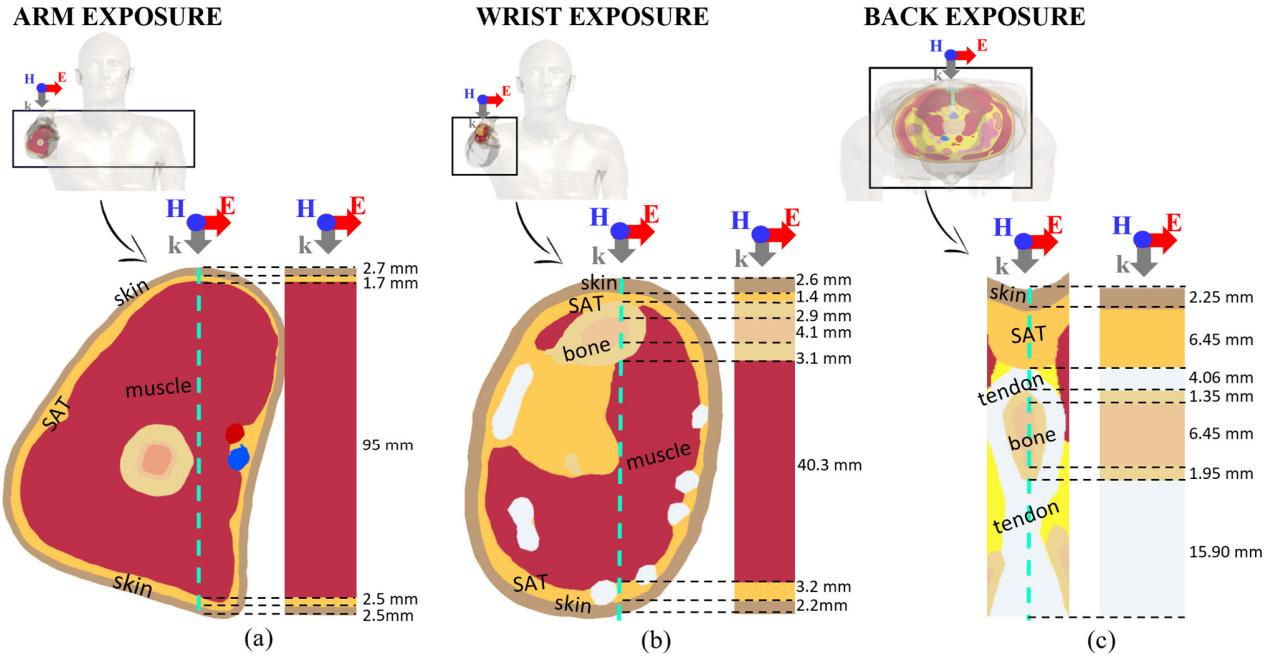

Fig. 2 Reference body section selected for the comparison and the construction of the "Duke-specific" multilayer planar slab for the (a) arm, (b) wrist and (c) back. The arrows represent the triads E-H-k of the k-impinging plane wave. The dotted cyan line identified the reference tissue sequence encountered by the plane wave impinging normally to the air/skin interface. Each tissue is identified in the figure by a label.

stratum corneum, epidermis&dermis (that are electromagnetically equivalent), and fat.

At frequencies below 30 GHz, a four layers body model is preferred, to account for extracutaneous tissues, usually modelled as muscle. While there is some accordance in the number of layers chosen to model the body, there is still high variability in the chosen thicknesses, that depend on the body part taken into account. Hence, we moved from this overview to reproduce a typical body model to study at 24 GHz, to allow comparison with literature data as well as with currently available virtual human phantoms. This multilayer slab model is described in Section III B.

III. Comparison Between Multilayer Slab and Anthropomorphic Model

A. Plane Wave Exposure of the 3D Realistic Model

Duke model from the Virtual Population (ViP 3.0 [27]) was used as the 3D realistic model (Fig. 1).

Duke is a whole-body male model representing a standard Caucasian man (34 years old, 1.77 m high and 77 kg of weight). As all the ViP models, it was obtained from MRI data of an healthy volunteer using a scanning resolution of $0.9 \times 0.9 \times 2$ mm^3 in the torso and limbs [27]. The model counts

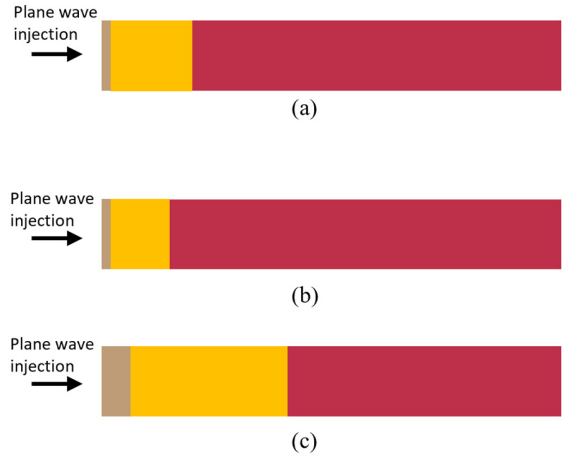

Fig. 3 "Literature-generic" slabs typical of (a) the arm, (b) the wrist, (c) a generic body district. Tissues are represented by color. Skin: ocher, SAT: yellow, Muscle: red.

TABLE II
GEOMETRICAL AND DIELECTRIC PROPERTIES OF LITERATURE-GENERIC SLABS

Tissue	Thickness (mm)	Dielectric properties [44]
Viable epidermis and dermis	1.2 (a,b) or 1.5 (c)	18.96-j17.1
Fat	8 (a) or 4 (b) or 14 (c)	6.50-j3.31
Muscle	∞	27.34-j21.96

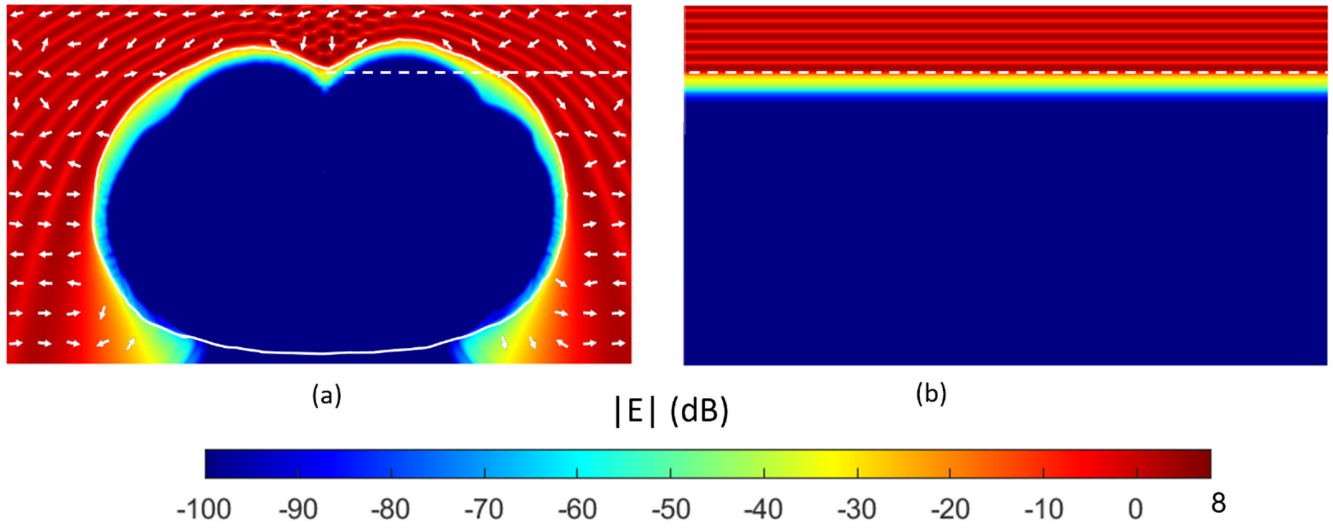

Fig. 4 Comparison between the E-field maps inside and around (a) the anthropomorphic back and (b) its Duke-specific slab. This was obtained with planar 2D solution, extended along the dimension of the entire 3D simulation. The white arrows show direction and orientation of the external E-field due to the stationary wave. The white lines indicate the skin/air interface in both panels.

for a total of 305 separated body structures, grouped in 38 electromagnetically different tissues. The tissue flagged in Duke as skin accounts for the layer of epidermis&dermis, with an average thickness in line with [23] while the subcutaneous adipose tissue (SAT) is separately represented. In this work, the electromagnetic properties, corresponding to the real part of the equivalent conductivity (i.e., σ) and the real part of the complex permittivity (i.e., ε_r), were assigned to each tissue from the IT'IS Database at the frequency of interest, i.e. 24 GHz [45] Particularly, the skin and SAT characteristics assigned by default to the ViP models correspond to those of the dry skin and the infiltrated fat from [46], and they are in line with properties assigned to several slab models [20], [39]–[41]. As shown by the three panels of Fig.1, rather than a whole-body investigation, we focused on three different body parts, separately: the arm (Fig. 1a), the wrist (Fig. 1b) and the back (Fig. 1c). Each one was exposed to an incident plane wave at 24 GHz, that propagated perpendicularly to its longitudinal axis (Fig. 1). Such polarization was named *impinging k* and was characterized by the triple E-H-k shown in Fig. 2. Three separate EM simulations were performed all using the high frequency solver of the simulation software Sim4Life, v.6 (Zurich MedTech AG, Zurich), that implements the FDTD method. A non-uniform mesh with a minimum step of 0.1 mm in the anatomic area of interest and a maximum of 0.87 mm at the borders was chosen to discretize the three simulation domains, resulting in a total of 2.3 GCells, 1.12 Gcells and 655 MCells for arm, wrist and back, respectively. Absorbing boundary conditions were set using 10 layers of PML (perfectly

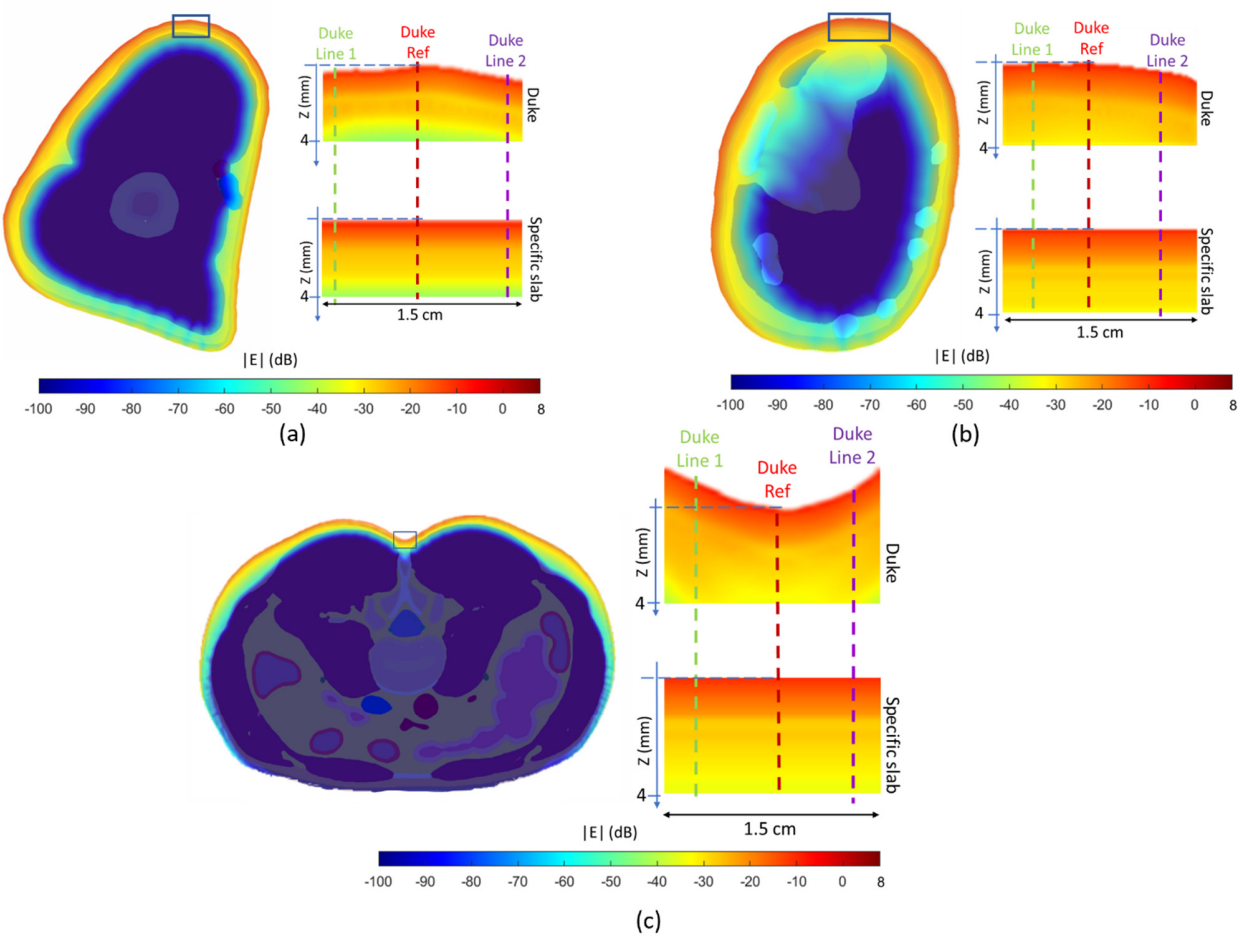

Fig. **5** Detail of the E-field maps inside the tissues (left subpanel) and in a region of interest down to 4 mm inside the Duke and the specific slab models (right subpanel) for exposure of the (a) arm, (b) wrist and (c) back. In the left subpanel the E-field distribution is superimposed to the tissue composition and the region of interest is identified by the blue square. In the right subpanel: is the region of interest. Red dotted line identifies the position of the reference tissue sequence. Green and purple dotted lines identifies two locations of interests inside the models, named Duke Line 1 and Duke Line 2.

matched layer) material and 20 cells of free space were added around the voxel domain.

All the simulations ran on a workstation AMD Ryzen 9 5950X 16-Core Processor @3.40 GHz, RAM 128 GB, with a mounted graphical card NVIDIA GeForce RTX3060. For a faster computational time, the Sim4Life GPU accelerator Axware was used and the maximum computational time was 10 hours.

B. Plane Wave Exposure of the Multilayer Slabs

Six different multilayer slabs were created to be compared with Duke's body parts. The first set of three models were built to reproduce the reference section of the corresponding body part, so to create an equivalent planar model of Duke, as shown in Fig. 2. Such section was chosen as the most representative of the heterogeneous and non-planar characteristics of the realistic model. These equivalent planar models were defined as *Duke-specific* slabs, and will be referred to as specific slabs, for simplicity. The considered refence section is identified in Fig. 1 by the blue plane and shown in detail in Fig. 2. For each specific slab, the distribution and thicknesses were derived from the stratification encountered in the anatomical model where the direction of wave propagation is locally normal to the skin/air interface (cyan dotted line, Figure 2). In particular, the specific slab for the arm was composed by 2.7 mm of skin, 1.7 mm of SAT, 95 mm of muscle, 2.5 mm of subcutaneous fat and 2.5 mm of skin. The specific slab for the wrist included 2.6 mm of skin, 1.4 mm of SAT, 2.9 mm of cortical bone, 4.1 mm of cancellous bone, 3.09 mm of cortical bone, 40.28 mm of muscle, 3.2 mm of SAT and 2.2 mm of skin. Finally, the specific slab for the back represented the first 4 cm of tissues and was composed by 2.25 mm of skin, 6.45 mm of SAT, 4.06 mm of tendon, 1.35 mm of cortical bone, 6.45 mm of cancellous bone, 1.95 mm of cortical bone and 15.9 mm of tendon. Three additional slabs were modeled, in accordance with the studies reported in Table I and described in Section II; they are referred as *literature-generic* slabs. The generic slabs all consisted in a layer of skin and fat, with typical thicknesses taken from literature, and a layer of muscle with a thickness properly selected to represent an infinite dimension along the propagation axis. Specifically, one consisted in a skin layer of

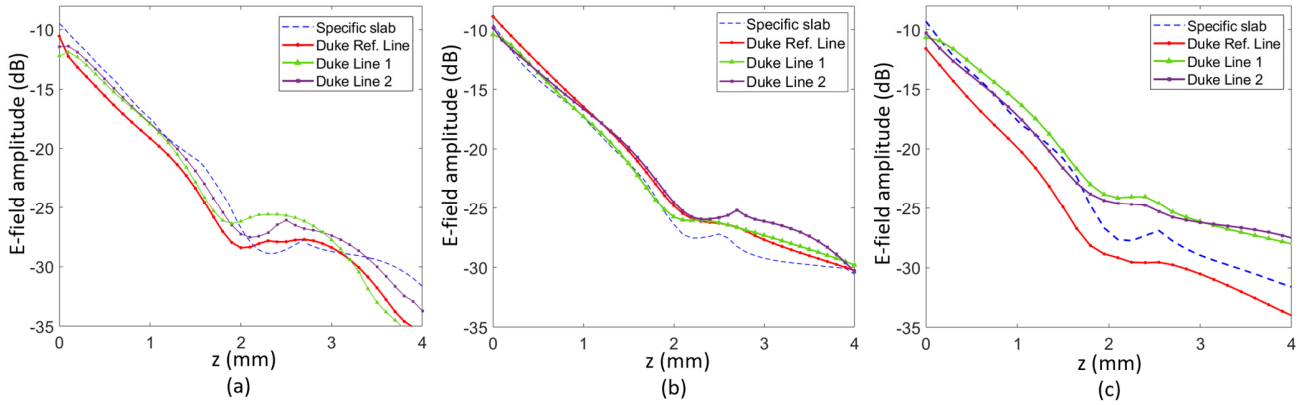

Fig. 6 Comparison between the E-field trend along the equivalent planar model (i.e., specific slab) and the three lines of interests in Duke: (a) arm, (b) wrist, (c) back.

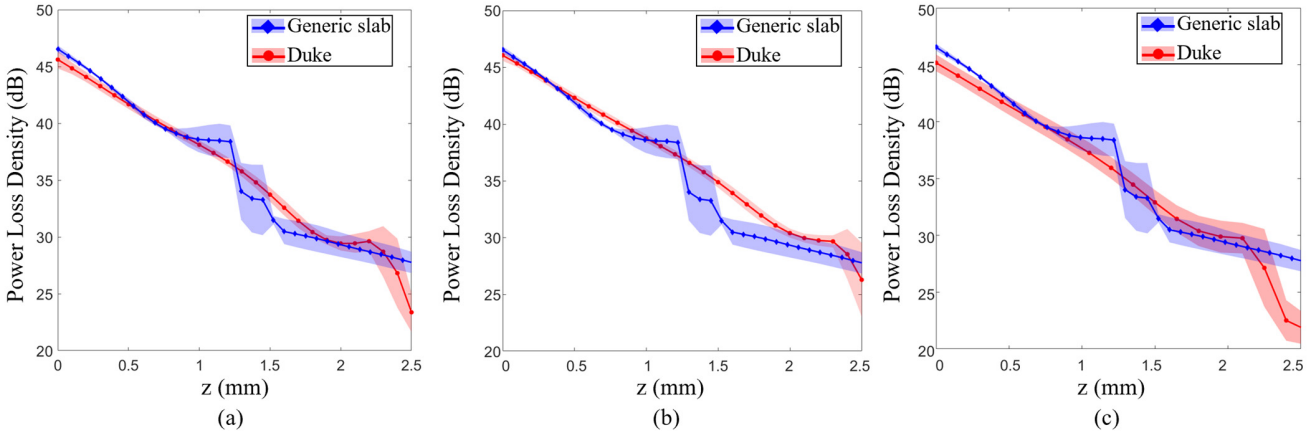

Fig. **7** Comparison of PLD trends between the generic slab and the Duke model for (a)arm, (b)wrist and (c)back. For the Duke model, the values are reported as mean (solid red) and standard deviation (shaded red area) inside the region of interest. For the generic slab, the values are reported as mean (solid blue) and standard deviation (shaded blue area) across the three models.

1.2 mm and a fat layer of 8 mm, and reproduced the characteristics of the arm according to [21] and [22]. The second, has a layering consisting of 1.2 mm of skin and 4 mm of fat and reproduced the characteristics of the wrist according to [21] and [22]. The third one had a layering composed of 1.5 mm of skin and 14 mm of fat and can be considered representative of a generic body part [21], [22]. Exposure of the three generic slabs is depicted in Fig. 3, and their characteristics are summarized in Table II. The layer of stratum corneum was not included because the exposure focused on body areas where it would be a thin layer of less than 20 μm, and its effect on the mmW power absorption would be therefore negligible [23], [41]. For both the specific and generic slab we flagged as skin the homogeneous layer of epidermis&dermis and we assigned the same dielectric properties assigned to the Duke model. This allowed accurate comparison between the modeling strategies investigated. The size of each surface normal to the direction of wave propagation is finite and is equal to a wavelength in air at 24 GHz, 1.25 cm. However, a combination of boundary conditions consisting of perfect Electric and perfect Magnetic wall was applied to all faces of the model so that surfaces perpendicular to the direction of wave propagation could be considered infinite in the two lateral dimensions.

IV. Results

A. Comparison With the "Duke-Specific" Multilayer Slab

Results of the electric (E-)field in the realistic model Duke are reported in Fig. 4a and Fig. 5, and were computed under the default settings of the simulation software, corresponding to an E-field intensity of 1 V/m, i.e., an incident plane of 1 mW. In Fig. 4a the distribution is along the reference plane of the back, both inside the tissues and in the outer free space. The presence of the non-planar incidence surface, offered by the back, reflected the plane-wave in different directions, causing interferences that locally change in the space, leading to a pattern that differs from that of a typical standing wave. For instance, a honeycomb pattern is created in correspondence of the dip, due to the reflections from the two side walls, that experience a locally oblique exposure. In that area, the peak of the combined wave reaches about 2.5 V/m (8 dB). Conversely, the reflections from the two humps have less interferences, resulting in a more regular pattern, and the maximum amplitude reached was about 1.5 V/m (3 dB). This behavior was confirmed by the direction of the external E-field, described by the white arrows, that locally changed their direction, with

TABLE III
E-FIELD VALUE AT THE SKIN-AIR INTERFACE AND AT 1 MM INSIDE THE SKIN.

	Specific slab		Duke Ref.		Duke Line 1		Duke Line 2	
	$E_{interface}$(dB)	$E_{z=1mm}$(dB)	$E_{interface}$(dB)	$E_{z=1mm}$(dB)	$E_{interface}$(dB)	$E_{z=1mm}$(dB)	$E_{interface}$(dB)	$E_{z=1mm}$(dB)
Arm	-9.47	-17.52	-10.54	-19.12	-12.19	-17.85	-11.45	-17.85
Wrist	-9.55	-17.33	-8.87	-16.44	-10.40	-17.28	-9.81	-16.62
Back	-9.30	-18.01	-11.59	-20.27	-10.67	-16.35	-10.29	-17.57

respect to the initial polarization. Furthermore, the side of the body is exposed as well offering an incidence surface (white solid line, Fig. 4a) oriented almost parallel to the propagation direction, albeit orthogonal to that of the electric field. This can be translated into a power absorption even in an area of the body that was not directly interested by the exposure, such as the hips. The maps of the E-field inside and around the back can be compared with the result obtained when implementing the analytical approach (Fig. 4b), by expanding the 1D solution in the 2D space, ensuring correspondence with the reference air/skin interface of the realistic model (white dotted line, Fig. 4). Conversely, the multilayer slab offered a planar surface orthogonal to plane wave propagation direction. Hence, in the space outside the tissues a perfect stationary wave is created as a combination of the incident and reflected waves. Similar considerations can be done for the wrist and the arm, whose E-field distributions are reported in the Supplementary Material and in Fig. 5. In these cases as well, the E-field streamlines were deformed by the curved surface offered by two targeted body parts and enclosed around them. The distribution inside the tissues followed a circular pattern around the entire perimeter of the arm and the wrist, with intensities that decrease in a radial direction. In both cases, inside the whole layer of skin, E-field intensity ranged from 0.33 V/m (-9.5 dB) to 0.01 V/m (-40 dB), for the *k-impinging* wave. Furthermore, Fig. 5 (left subpanels) also showed how the presence of different tissues composition influences the E-field distribution, particularly for the wrist characterized by the presence of many tissues.

The 3D realistic model was compared with the multilayer slabs over a 1.5 cm wide and 4 mm deep region of interest (ROI) inside the anatomical target (Fig. 5, right subpanels). Results showed the different E-field patterns, with the one inside Duke altered by the presence of several discontinuities with irregular interfaces. Taking into account the 1D nature of the slab, a further comparison was carried out over single lines extracted inside the realistic model, shown in Fig. 5: the red line is the one crossing the reference tissue sequence (i.e., Duke ref.), the green line was taken at -5 mm from Duke ref. (i.e., Duke Line 1) and the purple line was taken at +5 mm from Duke ref. (i.e.,Duke Line 2).

In Fig. 6 the trend along the slab is compared with that along the three lines inside Duke. The four curves obtained, including the specific slab and Duke Ref., differ from each other. Particularly, in all the body parts, the E-field inside Duke at the reference line, did not present the small peak that is visible in the specific slab at the interface between skin and SAT (~ 2.5 mm). Nevertheless, it could be found in Duke Line 2, although at a depth of 2.8 mm, due to the different position of the skin/SAT interface. Considering the exposure of the arm (Fig. 6a), the slab is not able to reproduce the trend obtained in the Duke model at any distance from the air/skin interface. As shown in Table III, the values estimated by the two methods differ by 1 dB (-9.47 dB for the specific slab and -10.54 dB for Duke Ref.) at the interface and by 2 dB at z=1 mm. The E-field of the SAT (z > 2 mm) decreases more slowly inside the slab than inside Duke, probably as an effect of the small curvature radius of the arm. Comparing the slab with Line 1 and 2, the differences at the interface are higher (up to almost 3 dB), but decrease towards z=1 mm, where a crossing point can be found. In the case of wrist exposure, the differences are lower, all below 1 dB. Higher values are estimated in Duke (Table III), and the values inside the SAT all decreased with similar a slope. Finally, the specific slab of the back overestimated the E-field intensities inside Duke Ref., with differences above 2 dB both at the interface and at z = 1 mm (Table III). Nevertheless, it could reproduce the trend of Duke Line 2, in the first millimeter of the skin, with a difference of 1 dB at the interface (-9.30 dB for the slab and -10.27 dB for Line 2) and 0.5 dB at 1 mm (-18.1 dB for the slab and -17.57 dB for Line 2). For Line 1 and Line 2, the E-field values inside the SAT were higher than in the other two cases, due to the influence of the tissues' sequence beyond 4 mm.

B. Comparison With the "Literature-Generic" Multilayer Slab

Results on the realistic 3D model Duke with those on the literature generic slabs were compared by considering the same plane wave propagation as in Section IIIA, but impinging with an input power density (IPD) of 31 W/m^2, which corresponds to the ICNIRP limit for local exposure at 24 GHz [15], [41], so to be in line with the analysis typically carried out by other studies performing computational dosimetry [16]. Furthermore, we considered the Power Loss Density (PLD) as the quantity of interest [29]. The results are shown in Fig. 7, where the PLD was reported in terms of average value (solid line) and standard deviation (shaded area). For the Duke model (plot in red), PLD was averaged inside the ROI described in Section IV A, and the standard deviation was considered to account for the variability due to the body characteristics in that area. Whereas, for the literature generic slabs (plot in blue), PLD was averaged across the three models, to reproduce the variability of the results available in the literature.

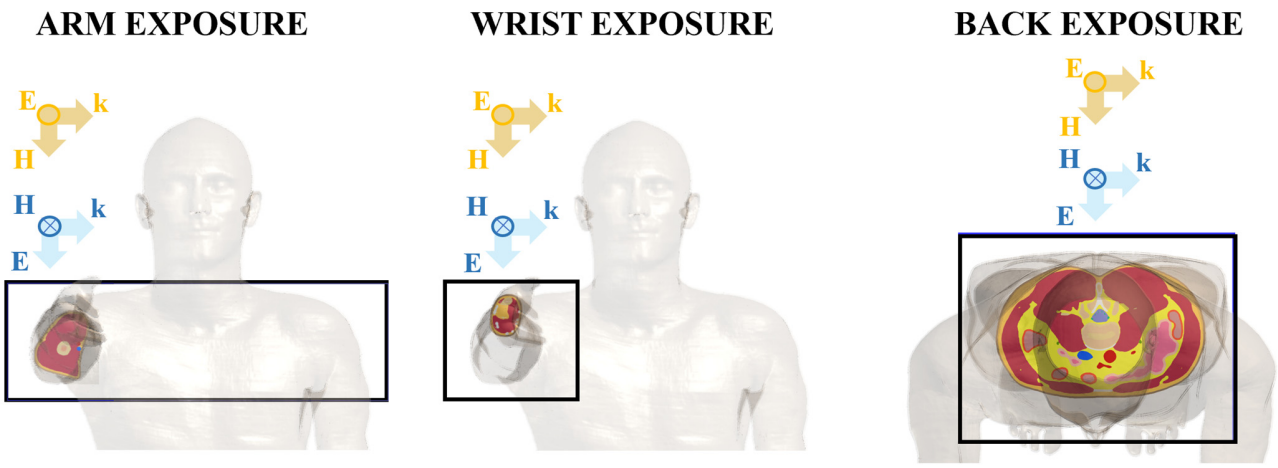

Fig.8 Exposure of (a) arm, (b) wrist and (c) back to different polarizations: impinging H (yellow) and impinging E (blue).

In the evaluated conditions, with an IPD of 31 W/m^2, the mean PLD value at the skin/air interface in Duke was 45.61 dB (36.4 kW/m^3) for the arm, 46.06 dB (40.4 kW/m^3) for the wrist and 45.17 dB (32.88 kW/m^3) for the back, that differed from the average value between the slabs by 0.9 dB for the arm, 0.5 dB for the wrist, and 1.4 dB for the back.

The standard deviation of the estimated PLD at the skin/air interface of the generic slab was ±0.31 dB, whereas it ranged between ±0.5 dB and ±0.78 dB for Duke. Inside the SAT, the maximum standard deviation was ±1.4 dB for generic slab, whereas it ranged between ±2.2 dB and ±3.4 dB in Duke.

C. Exposure of the Duke Model to Other Polarizations

One main limitation of using planar models for numerical dosimetry, is that it allows the study of a limited number of propagation direction [22], [26]. Particularly, incidence of plane waves travelling with a propagation direction parallel to the slab interfaces between the modelled tissues, cannot be investigated. Nevertheless, under this condition, either vector **E** or vector **H** can be impinging on the surface. It is expected that this different orientation of the tern E-H-k could lead to locally different exposure. To evaluate this aspect, we simulated the realistic model Duke under two further exposure conditions, i.e., one plane wave with impinging **E** (Pol_{iE}) and one with impinging **H** (Pol_{iH}). The respective terns are depicted in Fig. 8, for all the three body parts investigated in this study.

A local analysis was conducted, focused on the same ROI shown in Fig. 5 and described in Section III. The evaluated quantity was the induced E-field, and is reported in Fig. 9 as the mean (solid line) and standard deviation (shaded area) of the values averaged on the selected portion of the reference slice. While the trend followed by the mean E-field along the z axes is similar in the three propagation directions, for the three body parts, locally, a body section exposed to an impinging k plane wave experiences higher E-field values (i.e, -10.17 dB, -9.72 dB and -10.85 dB, at the air/skin interface for the arm, the wrist and the back, respectively). For Pol_{iE} the values dropped of by about 5 dB for the arm, 4 dB for the wrist and 15 dB for the back. For Pol_{iH} they dropped down by 13 dB, 15 dB and 30 dB. Furthermore, for the arm and the wrist, the two polarizations *iE* and *iH* lead to higher standard deviations in the first millimeter of skin, indicating a higher variability influenced by the tissue sequence encountered. For the arm, the standard deviation at the air/skin interface was 0.78 dB for *ik*, 1.33 dB for *iE* and 2.8 dB for *iH*. For the wrist, we had 0.5 dB for *ik*, 0.82 for *iE* and 2.56 dB for *iH*. Conversely, the standard deviation remained almost constant for the three polarizations in the back, with the minimum for the case *ik* (i.e., 0.67 dB vs 1.5 dB).

V. Discussion

The aim of this study was to conduct a comparison between two dosimetric approaches commonly used for computational dosimetry in the low range of the mmW frequencies (i.e., 24 GHz up to 28 GHz). At these frequencies, penetration depth, defined as the distance from the surface at which the absorbed power drops below 1/e, reaches 1 mm [16], which is comparable with the thickness of the skin. Hence, the skin is the most relevant tissue for dosimetry and a detailed representation is necessary for a good estimation of the exposure levels [16]. The skin is a heterogeneous multilayered tissue composed of a superficial layer of stratum corneum, with a low water content and a thickness below 20 µm for most body parts, a layer of viable epidermis and dermis, that have the same dielectric properties but different thermal characteristics, and characterized by an overall thickness as high as about 2.5 mm [16], [19]. Finally, a hypodermis layer made of subcutaneous adipose tissue is present. As a whole, the skin thickness can range from 1 mm to 3 mm [16], [19]. This stratified structure of the skin is what raised the concern about the most suitable body modelling strategy to be used in the mmW range. Indeed, in the range 24 GHz - 28 GHz the effect of internal reflection due to the interferences is not negligible and may still influence the exposure [16], [47]. Furthermore, it has recently been found that curved surfaces have an impact in the EM power absorption at these frequencies [29]. Hence, the literature is divided between the use of planar multilayer slabs [33], [37], [38], [48] and realistic 3D human models [33]–[35]. After two preliminary works that highlighted the differences between

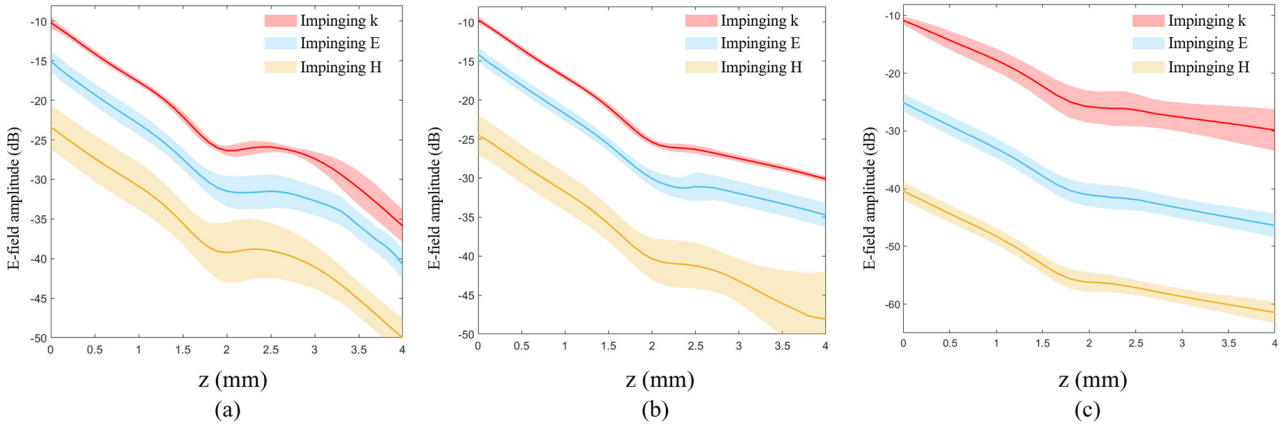

Fig. 9 Comparison of E-field trends between the three polarizations for (a)arm, (b)wrist and (c)back. The values are reported as mean (solid line) and standard deviation (shaded area) inside the region of interest.

dosimetric results estimated from a realistic 3D body model, selected as Duke from the ViP [27] and from multilayer planar slabs built *ad hoc* to reproduce Duke's wrist [30], [31] and Duke's abdomen [31], we continued the comparison focusing on highly non planar body parts, such as the arm, the wrist (when oriented with palm facing on one side), and the back.

We evaluated the exposure to a 24 GHz plane wave propagating along *z*, defined as the direction normal to the face of the planar model or to the longitudinal axis of Duke's selected body part. As previously done, the results were compared with *ad hoc* multilayer planar slabs, here in called *Duke-specific* slab, so to muffle the effect of the different tissues sequence encountered by the plane wave, and emphasize the differences due to curvature and to the presence of an heterogeneous distribution of the surrounding tissues. Furthermore, *Literature-generic* slabs were also considered, to compare results with the State-of-Art. When comparing the exposure estimated with the Duke model with those from the specific slab, both the absorbed power and the reflected E-field were evaluated.

As shown in Fig.4 and in Supplementary Figs. 1-3, the planar surface offered by the slab caused reflection of the wave along the same direction of the incident one, hence creating a stationary wave in the free space, with an E-field peak value twice as that of the impinging wave. Nevertheless, non-planar surface offered by some regions of the body, caused reflection in different directions, causing constructing or disrupting interferences, and generating unpredictable wave patterns around the body. This aspect influences the EM power absorbed inside nonplanar body parts, confirming what recently found in Sacco et al., 2022 [29], and might have an impact when evaluating the exposure of the human body with wearable or implanted devices [10].

Furthermore, comparison inside the tissues (Figs. 5-6 and Table III) demonstrated that the values estimated in the skin layer and already at the skin/air interface have differences ranging from 0.5 dB up to 2 dB, depending on the body part considered, contrary to what could be expected. Because the *Duke-specific* slabs perfectly reproduced the tissues sequence and thicknesses encountered by the wave inside the Duke model, such differences can be addressed to the internal reflections coming from the non-planar surfaces of Duke, as well as from surrounding tissues whose presence cannot be modelled by the planar slab.

The plots in Fig. 6 also showed how the tissue sequence beyond the penetration depth (i.e., 1 mm) can influence the values at more superficial levels. For instance, in the case of exposure of the back, the thickness of the skin between Duke Ref., Duke Line 1 and Duke Line 2 is the same, but in these latter cases the skin layer was followed by the tissue sequence SAT/fat (yellow tissue in Fig. 2), that is electromagnetically equivalent to a thicker layer of SAT. As a consequence, the induced E-field levels were higher in Line 1 and Line 2, than they were in the reference line at all distances from the interface. Interestingly, the specific slab reproduced the trend estimated by Line 2 in the first 1.5 mm of skin, but could not reproduce the trend in Duke Ref., from which the corresponding tissue sequence was extracted.

To compare the results estimated with the 3D realistic models with those obtained in literature, three multilayer planar model configurations were studied [21], [22].

To understand the consequences that the observed variations may have on thermal derived quantities, the results were compared in terms of power loss density for an incident input power density of 31 W/m^2 [15]. The differences in the values estimated at the skin/air interface were about the 60% of those obtained when considering the specific slab. Despite the operation of averaging the results, that is expected to muffle the dissimilarities between the two models, a non-negligible difference up to 1.5 dB still occurred, especially in case of misplacements of the skin/SAT interface. Furthermore, the standard deviation at the skin/air interface within the three generic slabs remained below 0.5 dB (Fig. 7). This confirmed that the results estimated by modelling the body with a planar surface are less sensitive to the tissue sequence, or to the layers' thickness. This would impact the evaluation of the absorbed power values with respect to anatomical or physiological variabilities of the skin, given the high variability of tissue thicknesses within the same person as well as among different subjects. Such variability is either in the thickness of the more

superficial layers of the skin and in that of the hypodermis layer, composed of SAT.

Finally, the use of 3D realistic human body models also allowed to evaluate exposure to plane wave travelling parallel oriented with respect to the surface of interest. Such condition cannot be taken into account with the planar strategy. Nevertheless, a parallel wave can lead to conditions that have either impinging electric field or impinging magnetic field in a given area of interest (Fig. 8). Despite a *k-impinging* wave seems to represent a worst case exposure scenario, always inducing higher values inside the first layer of skin (Fig. 9), it may be still relevant to consider a parallel travelling wave in case of exposure inside smart environments, where there could be multiple directions of incidence [10].

As a whole, the comparison conducted in the study highlighted that exposure results estimated with 3D realistic models or with multilayer planar slabs, have non-negligible differences that can be above 2 dB both at the interface, as well as inside the first 1 mm of skin layer, and in deeper regions. This would affects the results of a thermal analysis, where the heat propagates deeper than the EM power [29]. These results were derived considering a plane wave source in the three main polarization (k_i, E_i and H_i), corresponding to a far field exposure condition, however in several WPT and 5G application [4], [9] near field exposure to EM sources at the frequencies of interest of this study may occur, and we expect the differences between anthropomorphic and multilayer slab [38] models to be even more relevant.

It is important to highlight that the aim of this study was to evaluate the effect of neglecting body shape and anatomical details when estimating the exposure to EM sources in the low-band of the mmW spectrum. For seek of allowing the comparison with the ViP model Duke, the stratum corneum layer was not considered, following the stratification used in [21], [22]. Despite this approximation, the overall skin heterogeneity is preserved in the virtual model because the tissue flagged as *skin* represents the layer of epidermis&dermis, typically modeled as homogeneous in the electromagnetic solution. This is legit since this layer interfaces with the hypodermal fat (i.e., the SAT). Nevertheless, having separated skin layers remain a critical aspect to obtain an accurate numerical exposure assessment [38]. In fact, while epidermis and dermis, due to their similar water content, share the same EM properties, they have different ability to dissipate heat, because only the dermis is irrorated by blood vessels. As a result, distinct properties should be assigned to solve the thermal problem. Furthermore, at frequencies above 30 GHz, where the extracutaneous tissues have less influence in the power absorption, the presence of the stratum corneum may not be negligible. Hence, in the frequency range 24 GHz-28 GHz, the degree of detail of a virtual realistic model, in terms of both anatomical shape and tissue representation, make them suitable to give accurate estimation of the dosimetric EM solution quantities. Their use at frequencies above 30 GHz would require a separate modeling of stratum corneum, epidermis and dermis for an accurate numerical assessment of the exposure [49].

VI. Conclusion

This study highlighted the importance of considering the body anatomical shape when performing dosimetric evaluations on the exposure to EM sources in the low range of the mmW frequencies. The solution obtained with a 3D realistic model differed in a non-negligible way (up to 2 dB) from those obtained by both specific slabs and slabs typically used in literature and was more sensitive to changes in tissue sequence and thicknesses. Furthermore, the use of anthropomorphic models allows to study exposure to plane wave travelling in a parallel direction to the tissue surface, which is not possible with the planar approach. Hence, in the frequency range 24 GHz – 28 GHz the complexity of the human body should not be disregarded in favor of more simplified geometries. Nevertheless, before extending these results to frequencies above 30 GHz, it is important to highlight the limitation regarding the absence of separate layers of stratum corneum, dermis and epidermis, and future realistic body models for computational exposure assessment should be realized with novel techniques that allow to discriminate the complex structure of the skin tissue.

Acknowledgment

Authors wish to thank ZMT Zurich MedTech, AG for providing licenses of the simulation software Sim4Life.

References

[1] A. Costanzo *et al.*, “Electromagnetic energy harvesting and wireless power transmission: A unified approach,” *Proc. IEEE*, vol. 102, no. 11, pp. 1692–1711, Nov. 2014.

[2] Z. Zhang, H. Pang, A. Georgiadis, and C. Cecati, “Wireless Power Transfer - An Overview,” *IEEE Transactions on Industrial Electronics*, vol. 66, no. 2. Institute of Electrical and Electronics Engineers Inc., pp. 1044–1058, 01-Feb-2019.

[3] N. Shinohara, “History and Innovation of Wireless Power Transfer via Microwaves,” *IEEE J. Microwaves*, vol. 1, no. 1, pp. 218–228, Jan. 2021.

[4] A. Costanzo and D. Masotti, “Energizing 5G: near- and far-field wireless energy and data trantransfer as an enabling technology for the 5G IoT,” *IEEE Microw. Mag.*, vol. 18, no. 3, pp. 125–136, May 2017.

[5] S. R. Khan, S. K. Pavuluri, G. Cummins, and M. P. Y. Desmulliez, “Wireless power transfer techniques for implantable medical devices: A review,” *Sensors (Switzerland)*, vol. 20, no. 12. MDPI AG, pp. 1–58, 01-Jun-2020.

[6] B. Clerckx, R. Zhang, R. Schober, D. W. K. Ng, D. I. Kim, and H. V. Poor, “Fundamentals of wireless information and power transfer: From RF energy harvester models to signal and system designs,” *IEEE J. Sel. Areas Commun.*, vol. 37, no. 1, pp. 4–33, Jan. 2019.

[7] S. Ladan, S. Hemour, and K. Wu, “Towards millimeter-wave high-efficiency rectification for wireless energy harvesting,” in *2013 IEEE International Wireless Symposium, IWS 2013*, 2013.

[8] S. Ladan, A. B. Guntupalli, and K. Wu, “A high-efficiency 24 GHz rectenna development towards millimeter-wave energy harvesting and wireless power transmission,” *IEEE Trans. Circuits Syst. I Regul. Pap.*, vol. 61, no. 12, pp. 3358–3366, 2014.

[9] A. Costanzo *et al.*, “Wireless Power Transfer for Wearable and Implantable Devices: a Review Focusing on the WPT4WID Research Project of National Relevance.”

[10] A. Costanzo and D. Masotti, “Smart solutions in smart spaces,” *IEEE Microw. Mag.*, vol. 17, no. 5, pp. 30–45, 2016.

[11] S. S. Vinnakota, R. Kumari, H. Meena, and B. Majumder, “Rectifier Integrated Multibeam Luneburg Lens Employing Artificial Dielectric as a Wireless Power Transfer Medium at Mm Wave Band,” *IEEE Photonics J.*, vol. 13, no. 3, 2021.

[12] B. T. Malik, V. Doychinov, A. M. Hayajneh, S. A. R. Zaidi, I. D. Robertson, and N. Somjit, “Wireless power transfer system for battery-less sensor nodes,” *IEEE Access*, vol. 8, pp. 95878–95887, 2020.

[13] H. Aliakbari, A. Abdipour, A. Costanzo, D. Masotti, R. Mirzavand, and P. Mousavi, "Far-Field-Based Nonlinear Optimization of Millimeter-Wave Active Antenna for 5G Services," *IEEE Trans. Microw. Theory Tech.*, vol. 67, no. 7, pp. 2985–2997, 2019.
[14] O. Galinina, H. Tabassum, K. Mikhaylov, S. Andreev, E. Hossain, and Y. Koucheryavy, "On feasibility of 5G-grade dedicated RF charging technology for wireless-powered wearables," *IEEE Wirel. Commun.*, vol. 23, no. 2, pp. 28–37, 2016.
[15] G. Ziegelberger *et al.*, "Guidelines for limiting exposure to electromagnetic fields (100 kHz to 300 GHz)," *Health Physics*, vol. 118, no. 5. pp. 483–524, 2020.
[16] A. Hirata *et al.*, "Human exposure to radiofrequency energy above 6 GHz: Review of computational dosimetry studies," *Physics in Medicine and Biology*, vol. 66, no. 8. IOP Publishing Ltd, 21-Apr-2021.
[17] K. R. Foster, M. C. Ziskin, and Q. Balzano, "Thermal Response of Human Skin to Microwave Energy: A Critical Review," *Health Phys.*, vol. 111, no. 6, pp. 528–541, 2016.
[18] K. R. Foster, M. C. Ziskin, and Q. Balzano, "Thermal modeling for the next generation of radiofrequency exposure limits: Commentary," *Health Phys.*, vol. 113, no. 1, pp. 41–53, 2017.
[19] J. C. J. Wei, G. A. Edwards, D. J. Martin, H. Huang, M. L. Crichton, and M. A. F. Kendall, "Allometric scaling of skin thickness, elasticity, viscoelasticity to mass for micro-medical device translation: From mice, rats, rabbits, pigs to humans," *Sci. Rep.*, vol. 7, no. 1, pp. 1–17, 2017.
[20] A. Kanezaki, S. Watanabe, A. Hirata, and H. Shirai, "Theoretical analysis for temperature elevation of human body due to millimeter wave exposure," in *2008 Cairo International Biomedical Engineering Conference, CIBEC 2008*, 2008.
[21] K. Sasaki, M. Mizuno, K. Wake, and S. Watanabe, "Monte Carlo simulations of skin exposure to electromagnetic field from 10 GHz to 1 THz," *Phys. Med. Biol.*, vol. 62, no. 17, pp. 6993–7010, 2017.
[22] K. Li, K. Sasaki, S. Watanabe, and H. Shirai, "Relationship between power density and surface temperature elevation for human skin exposure to electromagnetic waves with oblique incidence angle from 6 GHz to 1 THz," *Phys. Med. Biol.*, vol. 64, no. 6, 2019.
[23] A. Christ, T. Samaras, E. Neufeld, and N. Kuster, "Rf-induced temperature increase in a stratified model of the skin for plane-wave exposure at 6-100 ghz," *Radiat. Prot. Dosimetry*, vol. 188, no. 3, pp. 350–360, 2020.
[24] G. Sacco, S. Pisa, and M. Zhadobov, "Impact of Textile on Electromagnetic Power and Heating in Near-Surface Tissues at 26 GHz and 60 GHz," *IEEE J. Electromagn. RF Microwaves Med. Biol.*, vol. 5, no. 3, pp. 262–268, 2021.
[25] A. Hirata, D. Funahashi, and S. Kodera, "Setting exposure guidelines and product safety standards for radio-frequency exposure at frequencies above 6 GHz: brief review," *Ann. des Telecommun. Telecommun.*, vol. 74, no. 1–2, pp. 17–24, 2019.
[26] V. Anderson, R. Croft, and R. L. McIntosh, "SAR versus Sinc: What is the appropriate RF exposure metric in the range 1-10 GHz? Part I: Using planar body models," *Bioelectromagnetics*, vol. 31, no. 6, pp. 454–466, Sep. 2010.
[27] M. C. Gosselin *et al.*, "Development of a new generation of high-resolution anatomical models for medical device evaluation: The Virtual Population 3.0," *Phys. Med. Biol.*, vol. 59, no. 18, pp. 5287–5303, Sep. 2014.
[28] T. Nagaoka *et al.*, "Development of realistic high-resolution whole-body voxel models of Japanese adult males and females of average height and weight, and application of models to radio-frequency electromagnetic-field dosimetry," *Phys. Med. Biol.*, vol. 49, no. 1, pp. 1–15, Jan. 2004.
[29] G. Sacco, Z. Haider, and M. Zhadobov, "Exposure Levels Induced in Curved Body Parts at mmWaves," *IEEE J. Electromagn. RF Microwaves Med. Biol.*, vol. 6, no. 3, pp. 413–419, 2022.
[30] M. Colella, S. Di Meo, P. Marracino, M. Liberti, M. Pasian, and F. Apollonio, "Dosimetric Analysis of Plane Wave Propagation in Biological Tissues: Comparison Between Planar Multilayer vs Realistic Anatomical Models," in *2021 51st European Microwave Conference (EuMC)*, 2022, no. April, pp. 1034–1037.
[31] M. Colella, S. Di Meo, M. Liberti, M. Pasian, and F. Apollonio, "Numerical comparison of plane wave propagation inside realistic anatomical models and multilayer slabs," in *2022 52nd European Microwave Conference (EuMC)*, 2022, pp. 800–803.
[32] Y. Diao, E. A. Rashed, and A. Hirata, "Assessment of absorbed power density and temperature rise for nonplanar body model under electromagnetic exposure above 6 GHz," *Phys. Med. Biol.*, vol. 65, no. 22, 2020.
[33] R. Morimoto, A. Hirata, I. Laakso, M. C. Ziskin, and K. R. Foster, "Time constants for temperature elevation in human models exposed to dipole antennas and beams in the frequency range from 1 to 30 GHz," *Phys. Med. Biol.*, vol. 62, no. 5, pp. 1676–1699, 2017.
[34] I. Laakso, R. Morimoto, J. Heinonen, K. Jokela, and A. Hirata, "Human exposure to pulsed fields in the frequency range from 6 to 100 GHz," *Phys. Med. Biol.*, vol. 62, no. 17, pp. 6980–6992, 2017.
[35] M. S. Morelli, S. Gallucci, B. Siervo, and V. Hartwig, "Numerical analysis of electromagnetic field exposure from 5G mobile communications at 28 GHZ in adults and children users for real-world exposure scenarios," *Int. J. Environ. Res. Public Health*, vol. 18, no. 3, pp. 1–13, 2021.
[36] M. L. Yang *et al.*, "[The clinic experience of implantable diaphragm pacer in a patient with high cervical spinal cord injury and literature review].," *Zhonghua jie he he hu xi za zhi = Zhonghua jiehe he huxi zazhi = Chinese J. Tuberc. Respir. Dis.*, vol. 41, no. 9, pp. 718–723, Sep. 2018.
[37] T. Hamed and M. Maqsood, "SAR calculation & temperature response of human body exposure to electromagnetic radiations at 28, 40 and 60 GHz mmWave frequencies," *Prog. Electromagn. Res. M*, vol. 73, no. June, pp. 47–59, 2018.
[38] M. Bonato, L. Dossi, S. Gallucci, M. Benini, G. Tognola, and M. Parazzini, "Assessment of Human Exposure Levels Due to Mobile Phone Antennas in 5G Networks," *Int. J. Environ. Res. Public Health*, vol. 19, no. 3, 2022.
[39] A. Kanezaki, A. Hirata, S. Watanabe, and H. Shirai, "Effects of dielectric permittivities on skin heating due to millimeter wave exposure.," *Biomed. Eng. Online*, vol. 8, p. 20, 2009.
[40] T. Wu, T. S. Rappaport, and C. M. Collins, "Safe for generations to come: Considerations of safety for millimeter waves in wireless communications," *IEEE Microw. Mag.*, vol. 16, no. 2, pp. 65–84, 2015.
[41] G. Sacco, S. Pisa, and M. Zhadobov, "Age-dependence of electromagnetic power and heat deposition in near-surface tissues in emerging 5G bands," *Sci. Rep.*, vol. 11, no. 1, pp. 1–11, 2021.
[42] S. I. Alekseev and M. C. Ziskin, "Human skin permittivity determined by millimeter wave reflection measurements," *Bioelectromagnetics*, vol. 28, no. 5, pp. 331–339, 2007.
[43] S. I. Alekseev, A. A. Radzievsky, M. K. Logani, and M. C. Ziskin, "Millimeter wave dosimetry of human skin," *Bioelectromagnetics*, vol. 29, no. 1, pp. 65–70, 2008.
[44] M. C. Ziskin, S. I. Alekseev, K. R. Foster, and Q. Balzano, "Tissue models for RF exposure evaluation at frequencies above 6 GHz," *Bioelectromagnetics*, vol. 39, no. 3, pp. 173–189, 2018.
[45] P. Hasgall *et al.*, "IT'IS Database for thermal and electromagnetic parameters of biological tissues, Version 4.0," *IT'IS*, 2018. .
[46] S. Gabriel, R. W. Lau, and C. Gabriel, "The dielectric properties of biological tissues: II. Measurements in the frequency range 10 Hz to 20 GHz," *Phys. Med. Biol.*, vol. 41, no. 11, pp. 2251–2269, Nov. 1996.
[47] I. Laakso, R. Morimoto, A. Hirata, and T. Onishi, "Computational Dosimetry of the Human Head Exposed to Near-Field Microwaves Using Measured Blood Flow," *IEEE Trans. Electromagn. Compat.*, vol. 59, no. 2, pp. 739–746, 2017.
[48] W. He, B. Xu, M. Gustafsson, Z. Ying, and S. He, "RF Compliance Study of Temperature Elevation in Human Head Model Around 28 GHz for 5G User Equipment Application: Simulation Analysis," *IEEE Access*, vol. 6, pp. 830–838, 2017.
[49] Z. Haider, Y. Le Drean, G. Sacco, D. Nikolayev, R. Sauleau, and M. Zhadobov, "High-Resolution Model of Human Skin Appendages for Electromagnetic Dosimetry at Millimeter Waves," *IEEE J. Microwaves*, vol. 2, no. 1, pp. 214–227, 2021.

Micol Colella (Member, IEEE) received her Master's degree (cum laude) in Biomedical engineering and her PhD in Information and Communication Technology from Sapienza University of Rome in 2017 and in 2021, respectively. She's a currently holding a Postdoctoral research position in the BioEM Laboratory

at the Department of Information Engineering, Electronics and Telecommunication, Sapienza University of Rome.
From 2017, she's been involved in national and international projects in collaboration with industries and foreign research institutes. She is currently serving as Project Assistant for the EU-Funded Horizon 2020 Project RISEUP.
Her scientific interests include the computational modeling of electromagnetic fields interaction with the human body and dosimetry for clinical applications and safety purposes, with particular focus on neurostimulation and neuromodulation techniques, as well as 5G and WPT exposure systems. Dr. Colella is member of the BIOEM society, of the European Microwave Association (EuMA) and member of the URSI (International Union of Radioscience). She is Founder member of the Chapter Women In Radioscience (WIRS) Italy. In 2019 she was awarded with the Joseph Morissey Memorial Award for best platform presentation at the BioEM Joint Meeting. In 2021 she received the URSI GASS 2021 Young Scientist Award.

Simona Di Meo (Member, IEEE) was born in 1992. She received the M.Sc. degree (cum laude) in electronic engineering and the Ph.D. degree in electronics and computer science from the University of Pavia, Pavia, Italy, in 2016 and 2020, respectively. She is currently a Postdoctoral Researcher with Microwave Laboratory, Department of Electrical, Computer, and Biomedical Engineering, University of Pavia. Her current research interests include innovative techniques for early breast cancer detection. She was the Co-Principal Investigator (Co-PI) with the University of Pavia funding BlueSky Research Project MULTIWAVE.
She was the Education and research cooperation committee Chair and member of the Technical Program Committee for the Mediterranean Microwave Symposium 2022, and Student Activity Chair for the European Microwave Week 2022.
She is a member of the IEEE AP-S, MTT-S, EMB-S, WiE, the Italian Society on Electromagnetism (SIEm), and member of the National Group of Bioengineering (GNB). She was the recipient of several awards and recognitions, including the IEEE AP-S Eugene F. Knott Memorial Pre-Doctoral Research Award in 2015, the IEEE AP-S Doctoral Research Grant in 2018, the IEEE AP-S Fellowship in 2022, and several Young Scientist Awards in the framework of URSI conferences.
Dr. Di Meo is Associate Editor of the *IET Healthcare Technology Letters*.

Micaela Liberti (Senior Member, IEEE) received the M.Sc degree in electronic engineering and PhD from Sapienza University of Rome, Italy in 1995 and 2000, respectively. She is currently Associate Professor with the Department of Electronic Engineering, Sapienza University. From 2012 to 2015, she has been the national supplent representative of COST TD1104: "European network for development of electroporation-based technologies and treatments". In 2020 and 2021, she has being serving as President of the European Bioelectromagnetic Association (EBEA) and untill 2022 president ad interim of BioEM. Since 2021 she is member of the ICNIRP Scientific Expert Group and of the Technical Advisory Committee of URSI commission K. Since 2022 she is member of TC28 of IEEE-MTT Society. Her scientific interests include theoretical modeling in bioelectromagnetics, microdosimetry, exposure systems dosimetry and design.

Marco Pasian (Senior Member, IEEE) was born in 1980. He received the M.Sc. degree (cum laude) in electronic engineering and Ph.D. degree in electronics and computer science from the University of Pavia, Pavia, Italy, in 2005 and 2009, respectively. From 2004 to 2008, he spent periods at the European Space Agency, Germany, at Carlo Gavazzi Space, Italy, and at TNO, Defense, Security and Safety, The Netherlands. From 2009 to 2013 he held a post-doctoral position with the Microwave Laboratory, University of Pavia, where from 2013 to 2020 he was Assistant Professor. Since 2020, at the same institution, he is Associate Professor.
His research interests are in the field of microwave and mm-wave components, systems, and technologies, including substrate integrated waveguides, for space applications and investigation of complex, non-standard, media, most notably for biomedical imaging and cryosphere monitoring. Prof. Pasian has been Principal Investigator, or Unit Coordinator, for several competitive European and Italian grants. In addition, he has also been Project Manager, Scientific Manager, or Consultant for several projects in collaborations with European and Italian and European research centres and industries, including the European Space Agency.
Prof. Pasian is member of the European Microwave Association (EuMA) and member of the Italian Society on Electromagnetism (SIEm). He was the Technical Program Committee (TPC) Chair at the European Microwave Conference 2022, and served as TPC Co-Chair, TPC member, Conference Prize Committee Chair, and Finance Chair for other IEEE and EuMA conferences. He is Associate Editor of the *IEEE Journal of Electromagnetics, RF and Microwaves in Medicine and Biology* and Editor-in-Chief of the *EuMA International Journal of Microwave and Wireless Technologies*.

Francesca Apollonio (Senior member, IEEE) (M'06) received the PhD from Sapienza University of Rome, Italy in 1998. Since 2000, she joined the Department of Electronic Engineering, Sapienza University of Rome as Assistant Professor and since 2019 she is Associate Professor. Presently she is Chair of the

National Commission CNR-URSI, Commission K "Electromagnetics in Biology and Medicine" and since 2021 she has been elected Vice-Chair of the URSI International Commission K. Since 2020 she is member of the International Commission on Non-Ionizing Radiation Protection (ICNIRP) Scientific Expert Group. From 2016 to 2020 she has been National Representative for the Action COST CA15211. From 2015 to 2016 she has been Technical Program Committee Chair for the Annual Meeting of the Bioelectromagnetics Society (BEMS) and the European BioElectromagnetics Association (EBEA), BioEM2016. From 2012 to 2015, she served on the Board of Directors of the Bioelectromagnetic Society. She has authored more than 200 scientific publications on peer-reviewed international journals and conferences and chapter books. Her research interests include main aspects related to the interaction between electromagnetic fields and biological systems with reference to electroporation, smart drug delivery, molecular simulations of complex systems and exposure systems dosimetry and design.